Pis'ma v ZhETF, vol. 103, iss. 4, pp. 291 – 297 © 2016 February 25

Effect of magnetic order on the phase stability of the parent chalcogenide compound FeSe

S. L. Skornyakov[+*1)], *I. Leonov*[×], *V. I. Anisimov*[+*]

[+]*Institute of Metal Physics UB of the RAS, 620990 Yekaterinburg, Russia*

[*]*Ural Federal University, 620002 Yekaterinburg, Russia*

[×]*Theoretical Physics III, Center for Electronic Correlations and Magnetism, Institute of Physics, University of Augsburg, 86135 Augsburg, Germany*

Submitted 23 December 2015
Resubmitted 29 December 2015

We present results of first-principle calculation of the electronic structure and phase stability of the parent compound of Fe-based superconductors, FeSe, in a magnetically ordered state. In particular, we investigate ferromagnetic (FM) and two different types of antiferromagnetic (AFM) configurations (with magnetic structure vectors $(\pi, 0)$ and (π, π)). Our results for the total energy exhibit a two-minima shape for the FM and a standard parabolic-like behavior for the AFM configurations. We find a remarkable reconstruction of the electronic structure in the vicinity of the M point of the Brillouin zone which is accompanied with a rapid increase of magnetic moment upon expansion of the lattice volume. On that basis we propose that both the anomalous behavior of FeSe upon expansion of the lattice reported for the paramagnetic state (Phys. Rev. Lett. **115**, 106402 (2015)) and that obtained in the present work have a common origin.

DOI: 10.7868/S0370274X1604010X

Introduction. Since the discovery of superconductivity in iron-based oxypnictides [1], for almost a decade such materials have been at the focus of experimental and theoretical research [2–7]. These compounds are metals in the normal state and crystallize in a tetragonal structure where layers containing FeAs building blocks alternate with planes of other elements. It has been well-established that the electronic and transport properties of the FeAs systems, including superconductivity, are associated with the Fe atoms. The electronic states originating from other elements give a minor contribution at the Fermi surface. In that respect, understanding of mechanisms that lead to superconductivity requires a "minimal model" compound which shows all characteristic features of multicomponent Fe-based superconductors and, at the same time, has the simplest crystal structure.

Recently, superconductivity has been reported in the iron chalcogenide compound FeSe with $T_c \sim 8\,\mathrm{K}$ [8]. It has been discovered that the critical temperature can be enhanced up to 37 K under pressure [9–11]. The compound is the end member of the FeSe(Te) family (the so-called "11" type compounds) and can be regarded as a parent material for all Fe-based superconductors due to simplicity of its crystal structure which is reminiscent to that of the FeAs layers in the pnictides.

Band structure calculations [12–14], photoemission experiments [15–17] and magnetic measurements show that the electronic structure and magnetic properties of Fe-based chalcogenide superconductors in many aspects are similar to those of pnictides. In particular, the Fermi surface of FeSe possesses a $\mathbf{Q} = (\pi, \pi)$ nesting [18, 19], in agreement with the magnetic measurements performed at about T_c [20–23]. However, unlike to pnictides, which in normal state are spin-density-wave antiferromagnets, FeSe shows no static magnetism. By contrast, the isostructural compound FeTe which shows no superconductivity at ambient pressure is antiferromagnic with a propagation vector $(\pi, 0)$.

It is known that doping as well as external pressure can influence or even induce superconductivity in the pnictogen-based compounds. In the case of FeSe(Te), the T_c is sensitive not only to pressure but also to chemical (isovalent) doping which is untypical for pnictides. In particular, partial substitution of Se with Te increases T_c up to $\sim 14\,\mathrm{K}$ in $FeSe_{1-x}Te_x$ with $x \sim 0.5$ [24, 25]. Such substitution can be regarded as a negative pressure (expansion of the lattice) due to a larger ionic radius of Te compared to that of Se. We note that FeTe, i.e., another end member of the "11" family, shows a

[1)]e-mail: skornyakov@imp.uran.ru

Fig. 1. FeSe AFM configurations studied in the present work: Double-stripe configuration with propagation vector $(\pi, 0)$ (left) and single-stripe configuration with $\mathbf{Q} = (\pi, \pi)$ (right). Shaded areas show the magnetic unit cells

pressure-induced transition to a low-volume tetragonal phase which is accompanied with a collapse of local moments. However, superconductivity in that compound does not emerge even at pressures as high as 19 GPa [26].

The interplay of electronic and magnetic degrees of freedom in FeSe(Te) has been addressed in several papers. Ciechan and coauthors [27] investigated the effect of the *ab*-plane strain and hydrostatic pressure on the magnetic structure of FeTe. Employing density functional theory (DFT) they studied the stability of different magnetic orderings of Fe moments under various stress conditions. The effect of magnetic order on the electronic structure of FeSe has been also studied by Shi and Li and coauthors [28, 29] within DFT. Leonov and coauthors [30] have investigated structural phase stability of paramagnetic FeSe using a combination of density functional theory and dynamical mean-field theory (DFT+DMFT). They predict that FeSe undergoes a phase transition to a metastable high-volume tetragonal phase and show that such an unusual behavior is connected to a correlation-induced local moment formation caused by a shift of the van Hove singularity at the M point of the Brillouin zone.

In this Letter, we extend our previous study [30] of the electronic and structural properties of paramagnetic FeSe to a magnetically ordered state. In particular, we study the structural stability and magnetic properties of FeSe in two antiferromagnetic (AFM) configurations relevant for superconductivity and in the ferromagnetic (FM) state. Our results demonstrate that static magnetization alone treated within DFT cannot give a satisfactory description of the equilibrium volume and elastic properties of FeSe, indicating a crucial role of Coulomb correlations. We also show that the mechanism explaining phase transition in paramagnetic FeSe upon lattice expansion can be also applied to the spin-polarized case.

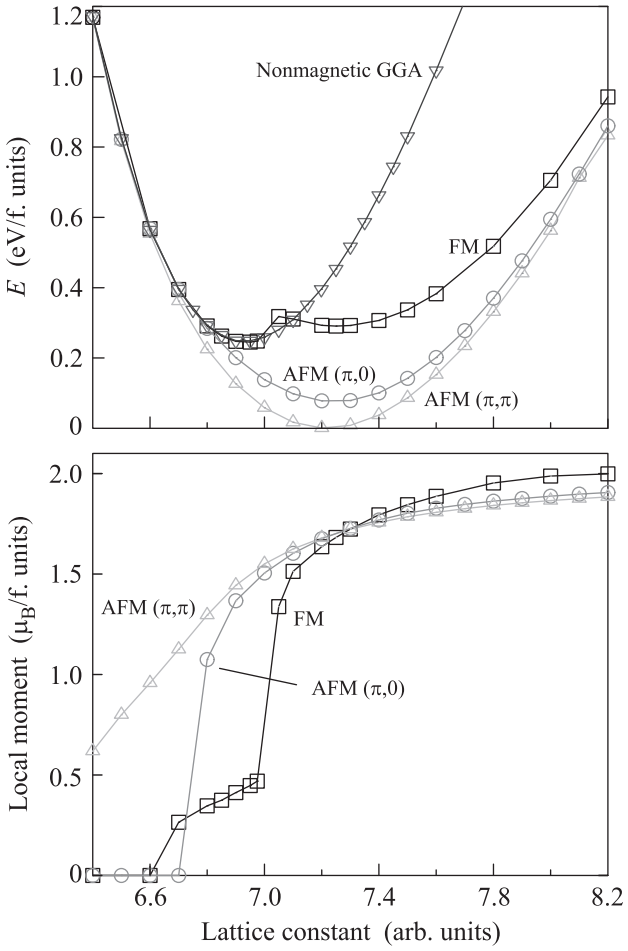

Fig. 2. Total energy (upper panel) and magnetic moment per formula unit (lower panel) calculated by GGA as a function of lattice volume

Calculation details. The effect of hydrostatic pressure in a magnetically ordered phase was studied by employing density functional theory in the generalized gradient approximation [31] as implemented in the pseudopotential plane-wave quantum ESPRESSO code [32]. Integration over the first Brilloiun zone (BZ) was performed using the uniform $10\times10\times10$ k-points mesh and default parameters controlling the plane wave basis. We study the phase stability analyzing the total energy behavior as a function of lattice volume. The compressibility is assumed to be isotropic, therefore only a single structural parameter a referred to as a lattice constant is needed to vary the lattice volume at fixed c/a ratio. We investigate the tetragonal phase of FeSe with the space group $P4/nmm$ and lattice parameters taken from Ref. [33]. The calculated AFM configurations of FeSe are shown in Fig. 1. The double-stripe AFM configuration corresponding to the propagation vector $(\pi, 0)$ is described by an orthorhombic magnetic unit

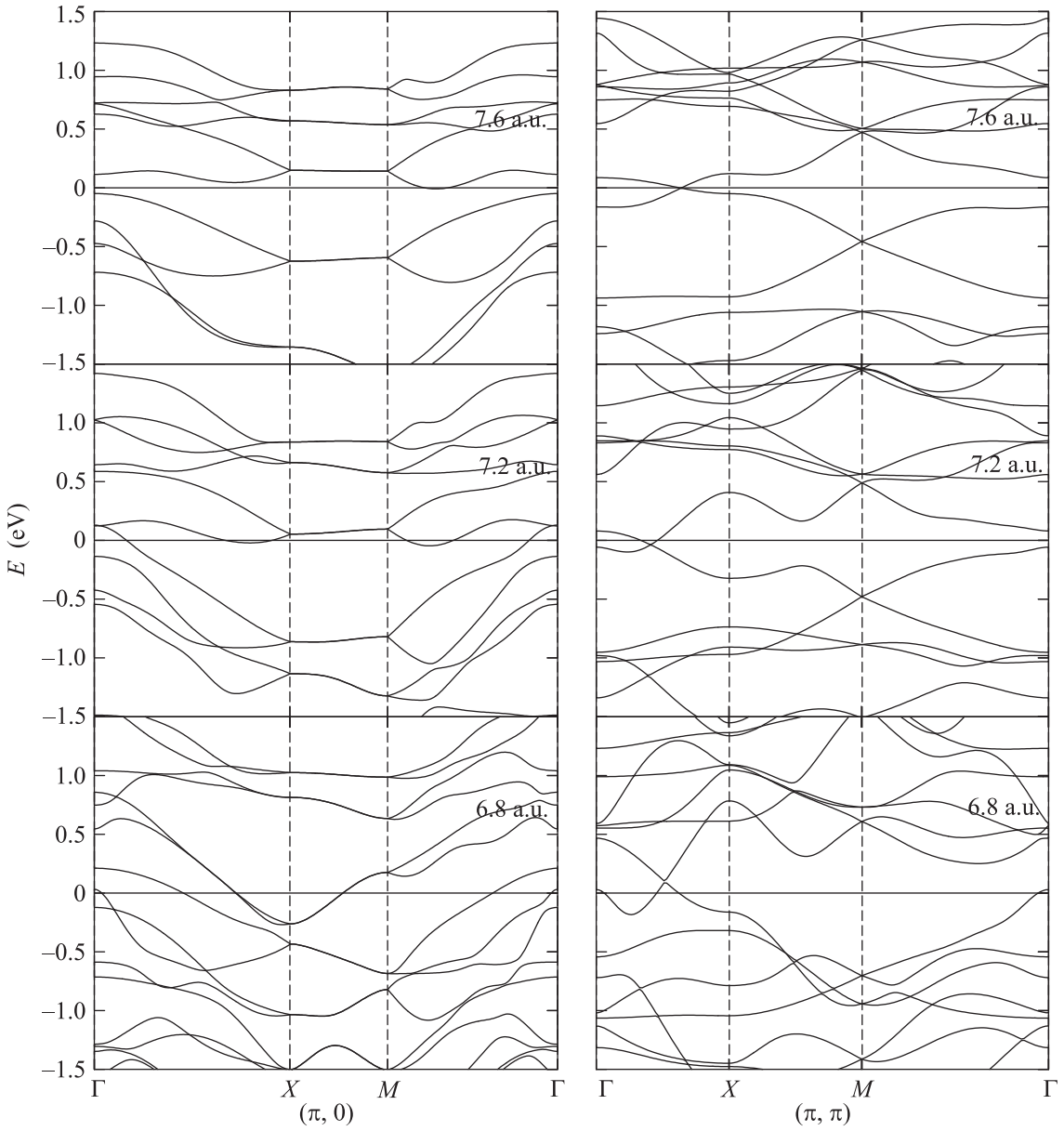

Fig. 3. Band structure of FeSe along the $\Gamma-X-M-\Gamma$ path in the Brillouin zone as obtained by spin-polarized GGA for different lattice constants and antiferromagnetic orderings of the Fe atoms. Left panels show the result for $(\pi, 0)$ AFM configuration, right panels correspond to the (π, π) type antiferromagnetism

cell $2a \times a \times c$. The stripe-diagonal AFM configuration has a tetragonal magnetic unit cell $a\sqrt{2} \times a\sqrt{2} \times c$ and $\mathbf{Q} = (\pi, \pi)$. For each considered magnetic configuration we extract the equilibrium bulk modulus B by fitting the obtained energy-volume dependence by the third-order Birch–Murnaghan equation of state [34].

Results and discussion. In Fig. 2 (upper panel) we present our results for the total energy of FeSe evaluated as a function of lattice volume. In agreement with previous studies, the nonmagnetic (NM) calculations underestimate the equilibrium lattice constant by 3 % compared to experiment. The calculated bulk modulus is $B \sim 115$ GPa. The AFM configurations show a standard parabolic-like behavior with a minimum at ~ 7.2 arb.units overestimating the experimental lattice constant by ~ 1 %. The calculated bulk moduli for the $(\pi, 0)$ and (π, π) configurations are 47 and 54 GPa, respectively. These values are compatible to those which are typical for the iron-based superconductors [35, 36]. In contrast to the NM and AFM result, the FM configuration has two well-defined minima with a transition region at ~ 7 arb.units. The stable solution (which

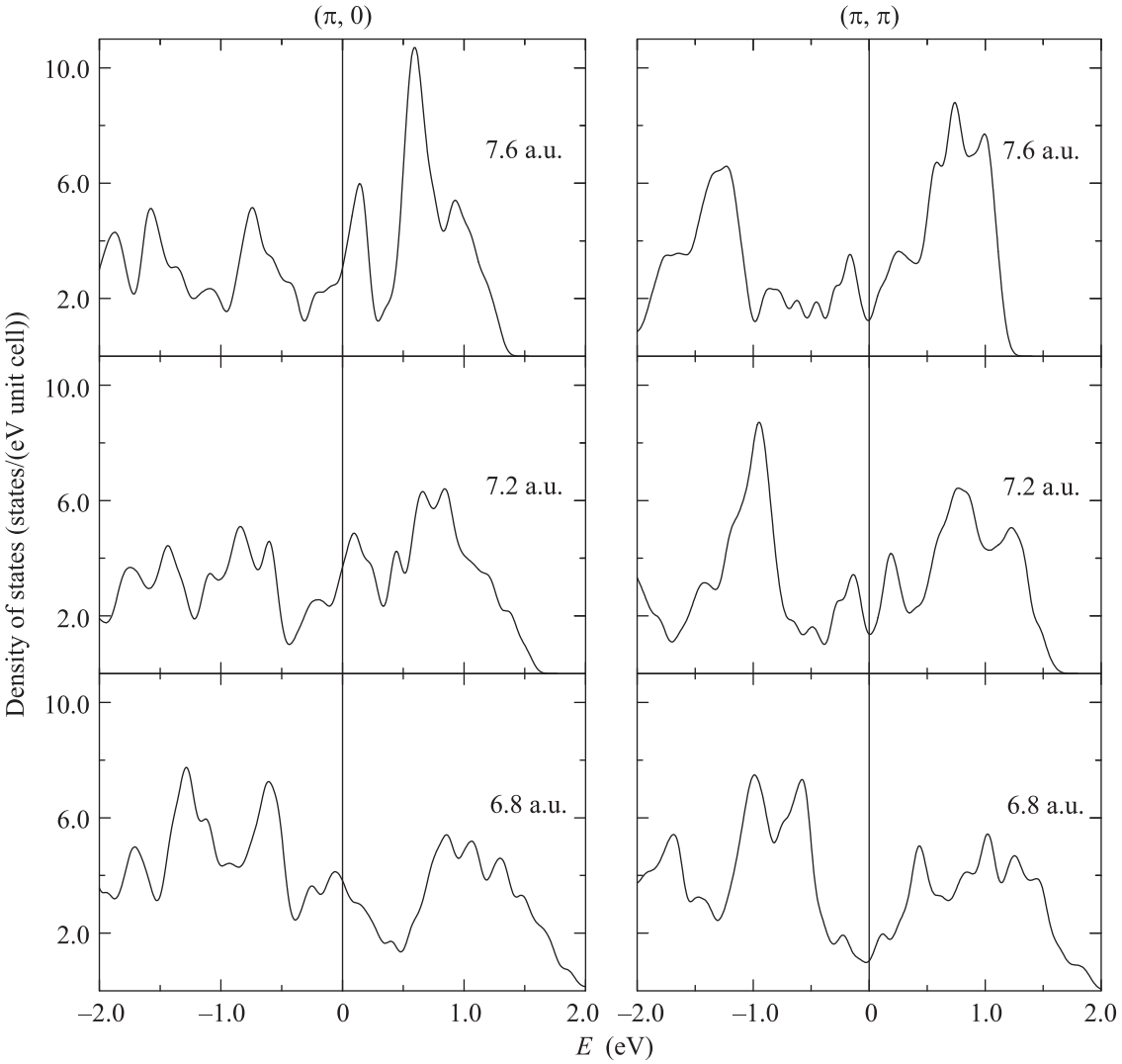

Fig. 4. Density of states of FeSe calculated by GGA for the $(\pi, 0)$ (left) and (π, π) (right) AFM configurations as a function of lattice volume. The Fermi energy is shifted to 0 eV

we refer to as a left minimum) has the lattice constant value of 6.9 arb.units, which is almost coincide with that obtained for the NM state. It results in much harder lattice with $B \sim 155$ GPa. The second metastable solution (right minimum) has $a \sim 7.3$ arb.units which is by 3 % lager than the experimental value. The bulk modulus is ~ 35 GPa which is much smaller than any available experimental data.

In spite that none of the considered static magnetic configurations treated within DFT give a simultaneous description of the structural and elastic properties of FeSe, our results are important to reveal a microscopic origin of this unusual double-minimum behavior. We also note that previous calculations of the paramagnetic (PM) FeSe within dynamical mean-field theory give a similar result. The origin of that behavior has been traced to a Lifshitz transition caused by a correlation-induced shift of the van Hove singularity at the M point of the BZ which is accompanied with a strong enhancement of the local magnetism. Similar to DFT+DMFT, the magnetic moment in the AFM and FM configurations increases upon expansion of the lattice, reaching its saturated value of $\sim 2\mu_{\mathrm{B}}$ per formula unit. Below $a \sim 6.6$ arb.units the magnetic and nonmagnetic solutions are energetically indistinguishable. At higher volumes the solution corresponding to the (π, π) ordering has the lowest energy showing a smooth increase of magnetization upon lattice expansion. For the $(\pi, 0)$ configuration, the total energy is lower than that in the NM case starting from $a \sim 6.7$ arb.units demonstrating rather rapid growth of the magnetic moment compared to the (π, π) case. The energy profile of the FM config-

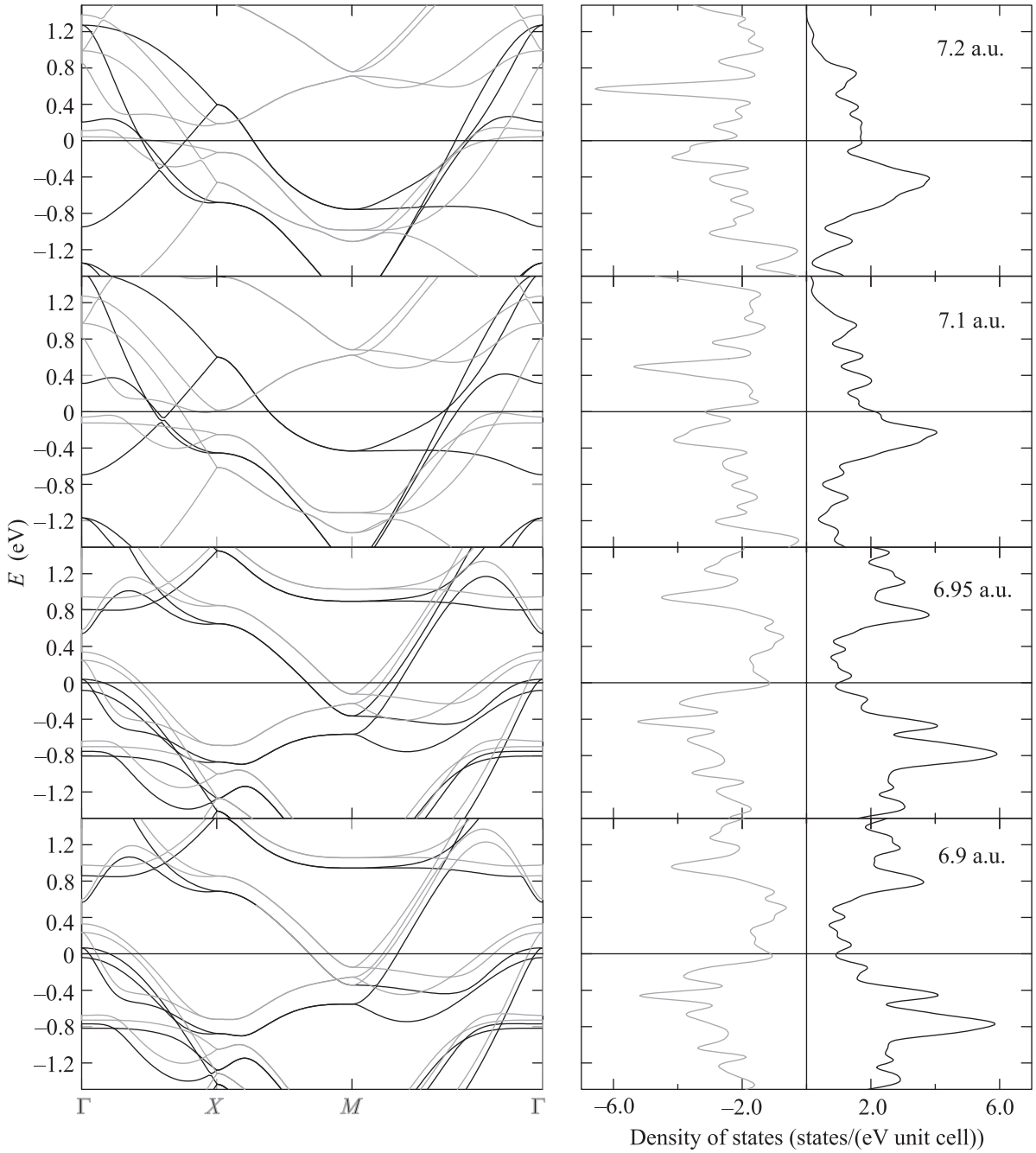

Fig. 5. Spin-polarized GGA results for FM FeSe computed for different lattice constants: Band structure (left panels) and density of states (right panels). Black and grey curves correspond to the spin projections. The Fermi energy is set to 0 eV

uration is very close to that of the NM solution up to $a \sim 7$ arb.units. Here the magnetization first shows a smooth increase in the vicinity of the left energy minimum then is followed by an abrupt jump which is located in the region separating the stable and metastable FM solutions.

In Fig. 3 we show the AFM band structure of FeSe calculated for the lattice volumes close to the equilibrium value. The corresponding densities of states are presented in Fig. 4. Overall shape of the dispersion curves and densities of states rather weakly depends on the lattice volume. The lattice constant variation mainly affects the band width and position of the Fermi level. This is connected with the charge transfer due to the change of hybridization between Fe-d and Se-p states. The shift of the Fermi energy is more pronounced in

the $(\pi, 0)$ case leading to a change of the Fermi surface along all high symmetry lines of the $\Gamma{-}X{-}M$ plane. For the (π, π) configuration, the change of the band structure and the densities of states is mainly a bandwidth effect. We note that in both AFM configurations the band structure at the M point, including the number of valence and conduction bands, remains unchanged.

In Fig. 5 we present the electronic structure calculated for the FM state. The FM ordering of Fe moments leads to a completely different band structure and its evolution upon variation of the lattice volume. In the vicinity of the left energy minimum the dispersion curves are very similar to those obtained in the NM and PM states (see Ref. [30]). The energy bands corresponding to different spin projections have similar shape and are shifted relatively to each other to yield a nonzero magnetization of the unit cell. Expansion of the lattice leads to a considerable reconstruction of the electronic structure in all regions of the $\Gamma{-}X{-}M$ plane, including the M point. In particular, as the lattice expands, flat bands at the M point in the energy interval $[-0.4, 0.0]$ eV shift towards the Fermi level. In the vicinity of the transition point (~ 7 arb.units) these bands are abruptly pushed to the energy interval $[0.4, 0.8]$ eV for one of the spin projections.

Our results reveal a similar behavior with that obtained for paramagnetic FeSe within DFT+DMFT. Namely, the FM result has a similar double-minimum shape for the total energy as that in DFT+DMFT. On the other hand, the total energy profiles calculated for the AFM configurations do not show that feature. Similarly to the DFT+DMFT results obtained for the PM state, the spin-polarized DFT yields a complete reconstruction of the electronic structure upon expansion of the lattice. However, the driving mechanism is different. Now it is mainly due to hybridization that controls a charge transfer. In the PM FeSe, the double minima feature originates from a Lifshitz transition that occurs due to a correlation-driven shift of the van Hove singularity at the M point above the Fermi level. Our DFT results show a significant change of the band structure at the M point only for the FM state where the total energy profile also has a double-minimum feature. On that basis we propose that an anomalous behavior of the total energy of FeSe upon variation of the lattice volume originates from a band structure reconstruction in the vicinity of the M point irrespective to a magnetic configuration.

The research was supported by the Russian Scientific Foundation (Project # 14-22-00004).

1. Y. Kamihara, H. Hiramatsu, M. Hirano, R. Kawamura, H. Yanagi, T. Kamiya, and H. Hosono, J. Am. Chem. Soc. **128**, 10012 (2006).
2. M. V. Sadovskii, Phys.-Usp. **51**, 1201 (2008).
3. J. Paglione and R. L. Greene, Nature Phys. **6**, 645 (2010).
4. D. N. Basov and A. V. Chubukov, Nat. Phys. **7**, 272 (2011).
5. G. R. Stewart, Rev. Mod. Phys. **83**, 1589 (2011).
6. P. Dai, J. Hu, and E. Dagotto, Nat. Phys. **8**, 709 (2012).
7. M. V. Sadovskii, E. Z. Kuchinskii, and I. A. Nekrasov, J. Mag. Magn. Mater. **324**, 3481 (2012).
8. F. C. Hsu, J. Y. Luo, K. W. Yeh, T. K. Chen, T. W. Huang, P. M. Wu, Y. C. Lee, Y. L. Huang, Y. Y. Chu, D. C. Yan, and M. K. Wu, Proc. Natl. Acad. Sci. USA **105**, 14262 (2008).
9. Y. Mizuguchi, F. Tomioka, S. Tsuda, T. Yamaguchi, and Y. Takano, Appl. Phys. Lett. **93**, 152505 (2008).
10. S. Margadonna, Y. Takabayashi, Y. Ohishi, Y. Mizuguchi, Y. Takano, T. Kagayama, T. Nakagawa, M. Takata, and K. Prassides, Phys. Rev. B **80**, 064506 (2009).
11. S. Medvedev, T. M. McQueen, I. A. Troyan, T. Palasyuk, M. I. Eremets, R. J. Cava, S. Naghavi, F. Casper, V. Ksenofontov, G. Wortmann, and C. Felser, Nat. Mat. **8**, 630 (2009).
12. A. Subedi, L. Zhang, D. J. Singh, and M. H. Du, Phys. Rev. B **78**, 134514 (2008).
13. K.-W. Lee, V. Pardo, and W. E. Pickett, Phys. Rev. B **78**, 174502 (2008).
14. L. Zhang, D. J. Singh, and M. H. Du, Phys. Rev. B **79**, 012506 (2009).
15. K. Nakayama, T. Sato, P. Richard, T. Kawahara, Y. Sekiba, T. Qian, G. F. Chen, J. L. Luo, N. L. Wang, H. Ding, and T. Takahashi, Phys. Rev. Lett. **105**, 197001 (2010).
16. E. Ieki, K. Nakayama, Y. Miyata, T. Sato, H. Miao, N. Xu, X.-P. Wang, P. Zhang, T. Qian, P. Richard, Z.-J. Xu, J. S. Wen, G. D. Gu, H. Q. Luo, H.-H. Wen, H. Ding, and T. Takahashi, Phys. Rev. B **89**, 140506(R) (2014).
17. K. Nakayama, H. Kim, T. Kawakami, Y. Nagai, T. Nakayama, X. Hu, Y. Hasegawa, and T. Uchihashi, Phys. Rev. Lett. **113**, 237001 (2014).
18. I. I. Mazin, D. J. Singh, M. D. Johannes, and M. H. Du, Phys. Rev. Lett. **101**, 057003 (2008).
19. A. V. Chubukov, D. V. Efremov, and I. Eremin, Phys. Rev. B **78**, 134512 (2008).
20. D. Christianson, E. A. Goremychkin, R. Osborn, S. Rosenkranz, M. D. Lumsden, C. D. Malliakas, I. S. Todorov, H. Claus, D. Y. Chung, M. G. Kanatzidis, R. I. Bewley, and T. Guidi, Nature **456**, 930 (2008).

21. M. D. Lumsden, A. D. Christianson, D. Parshall, M. B. Stone, S. E. Nagler, G. J. MacDougall, H. A. Mook, K. Lokshin, T. Egami, D. L. Abernathy, E. A. Goremychkin, R. Osborn, M. A. McGuire, A. S. Sefat, R. Jin, B. C. Sales, and D. Mandrus, Phys. Rev. Lett. **102**, 107005 (2009).
22. Y. M. Qiu, W. Bao, Y. Zhao, C. Broholm, V. Stanev, Z. Tesanovic, Y. C. Gasparovic, S. Chang, J. Hu, B. Qian, M. Fang, and Z. Mao, Phys. Rev. Lett. **103**, 067008 (2009).
23. M. D. Lumsden, A. D. Christianson, E. A. Goremychkin, S. E. Nagler, H. A. Mook, M. B. Stone, D. L. Abernathy, T. Guidi, G. J. MacDougall, C. de la Cruz, A. S. Sefat, M. A. McGuire, B. C. Sales, and D. Mandrus, Nat. Phys. **6**, 182 (2010).
24. B. C. Sales, A. S. Sefat, M. A. McGuire, R. Y. Jin, D. Mandrus, and Y. Mozharivskyj, Phys. Rev. B **79**, 094521 (2009).
25. A. Martinelli, A. Palenzona, M. Tropeano, C. Ferdeghini, M. Putti, M. R. Cimberle, T. D. Nguyen, M. Affronte, and C. Ritter, Phys. Rev. B **81**, 094115 (2010).
26. H. Okada, H. Takahashi, Y. Mizuguchi, Y. Takano, and H. Takahashi, J. Phys. Soc. Japan **78**, 083709 (2009).
27. A. Ciechan, M. J. Winiarski, and M. Samsel-Czekala, J. Phys. Cond. Mat. **26**, 025702 (2009).
28. Y.-F. Li, L.-F. Zhu, S.-D. Guo, Y.-C. Xu, and B.-G. Liu, J. Phys. Cond. Mat. **21** 115701 (2009).
29. H. Shi, Z.-B. Huang, J. S. Tse, and H.-Q. Lin, J. Appl. Phys. **110**, 043917 (2011).
30. I. Leonov, S. L. Skornyakov, V. I. Anisimov, and D. Vollhardt, Phys. Rev. Lett. **115**, 106402 (2015).
31. J. P. Perdew, K. Burke, and M. Ernzerhof, Phys. Rev. Lett. **77** 3865 (1996).
32. P. Giannozzi, S. Baroni, N. Bonini, M. Calandra, R. Car, C. Cavazzoni, D. Ceresoli, G. L. Chiarotti, M. Cococcioni, I. Dabo, A. Dal Corso, S. de Gironcoli, S. Fabris, G. Fratesi, R. Gebauer, U. Gerstmann, C. Gougoussis, A. Kokalj, M. Lazzeri, L. Martin-Samos, N. Marzari, F. Mauri, R. Mazzarello, S. Paolini, A. Pasquarello, L. Paulatto, C. Sbraccia, S. Scandolo, G. Sclauzero, A. P. Seitsonen, A. Smogunov, P. Umari, and R. M. Wentzcovitch, J. Phys.: Cond. Mat. **21** 395502 (2009); Homepage of Quantum ESPRESSO code: www.quantum-espresso.org.
33. M. C. Lehman, A. Llobet, K. Horigane, and D. Louca, J. Phys.: Conf. Ser. **251**, 012009 (2010).
34. F. Birch, Phys. Rev. **71**, 809 (1947).
35. G. Garbarino, P. Toulemonde, M. Álvarez-Murga, A. Sow, M. Mezouar, and M. Núñez-Regueiro, Phys. Rev. B **78**, 100507(R) (2008).
36. M. Mito, M. J. Pitcher, W. Crichton, G. Garbarino, P. J. Baker, S. J. Blundell, P. Adamson, D. R. Parker, and S. J. Clarke, J. Am. Chem. Soc. **131**, 2986 (2009).